AD_____

Award Number: DAMD17-00-1-0406

TITLE: Detection of Breast Microcalcifications Under Ultrasound Using Power Doppler and Acoustic Resonance Imaging

PRINCIPAL INVESTIGATOR: Susan P. Weinstein, M.D.
Chandra Seghal, Ph.D.

CONTRACTING ORGANIZATION: University of Pennsylvania
Philadelphia, Pennsylvania 19104-3246

REPORT DATE: July 2002

TYPE OF REPORT: Annual

PREPARED FOR: U.S. Army Medical Research and Materiel Command
Fort Detrick, Maryland 21702-5012

REPORT DOCUMENTATION PAGE

Form Approved
OMB No. 074-0188

1. AGENCY USE ONLY (Leave blank)	2. REPORT DATE	3. REPORT TYPE AND DATES COVERED
	July 2002	Annual (1 Jul 01 - 30 Jun 02)

4. TITLE AND SUBTITLE
Detection of Breast Microcalcifications Under Ultrasound Using Power Doppler and Acoustic Resonance Imaging

5. FUNDING NUMBERS
DAMD17-00-1-0406

6. AUTHOR(S)
Susan P. Weinstein, M.D.
Chandra Seghal, Ph.D.

7. PERFORMING ORGANIZATION NAME(S) AND ADDRESS(ES)
University of Pennsylvania
Philadelphia, Pennsylvania 19104-3246

E-Mail:weinstei@oasis.rad.upenn.edu

8. PERFORMING ORGANIZATION REPORT NUMBER

9. SPONSORING / MONITORING AGENCY NAME(S) AND ADDRESS(ES)
U.S. Army Medical Research and Materiel Command
Fort Detrick, Maryland 21702-5012

10. SPONSORING / MONITORING AGENCY REPORT NUMBER

11. SUPPLEMENTARY NOTES
report contains color

12a. DISTRIBUTION / AVAILABILITY STATEMENT
Approved for Public Release; Distribution Unlimited

12b. DISTRIBUTION CODE

13. Abstract *(Maximum 200 Words)* *(abstract should contain no proprietary or confidential information)*

Intraductal breast carcinoma (DCIS) represents approximately one third of mammographically detected breast carcinoma. Currently, DCIS and benign breast microcalcifications can only be reliably be evaluated utilizing x-ray mammography. Our goal with our current project was to utilize breast sonography coupled with the technique of acoustic resonance to image and evaluate the breast microcalcifications in patients prior to biopsy. We have been succesful in evaluating the calcifications. However, thus far, our analysis demonstrates no significant difference between the malignant and benign calcifications. Currently, work is ongoing with patient accrual.

14. SUBJECT TERMS	15. NUMBER OF PAGES
breast cancer, Doppler imaging, ultrasound, diagnosis, mammography	27
	16. PRICE CODE

17. SECURITY CLASSIFICATION OF REPORT	18. SECURITY CLASSIFICATION OF THIS PAGE	19. SECURITY CLASSIFICATION OF ABSTRACT	20. LIMITATION OF ABSTRACT
Unclassified	Unclassified	Unclassified	Unlimited

Table of Contents

Cover.....1

SF 298.....2

Table of Contents.....3

Introduction.....4

Body.....5-9

Technical Issues.....9

Key Research Accomplishments.....9-10

Reportable Outcomes.....10

Conclusions.....10-11

References.....12

Figures and Table.....13-19

Figure Legend.....20

Appendices.....21-25

Introduction:

Technical advances in the field of mammography are resulting in higher detection rate of early breast cancers than in the past, of both solid masses and microcalcifications. These technical advances include digital mammography, high frequency ultrasound transducers and breast magnetic resonance imaging (MRI). Mammography is still the only reliable method of evaluating microcalcifications in the breast. Breast MRI, although has a sensitivity rate nearing 100% for invasive carcinoma, the reported sensitivity for DCIS has been reported to be as low as 40% (1-3). It is estimated that DCIS represents 20-30% of breast carcinomas detected on screening mammography (4) and has been steadily been rising in incidence since the 1970's (5). Our goal is to image breast microcalcifications utilizing sonography, a readily available equipment in breast imaging centers, coupled with acoustic resonance. The concept of acoustic resonance imaging (ARI) is based on the size of the microcalcifications and the binding strength with the surrounding tissues in which it is imbedded. When subjected to a wide frequency range, different sized particles will resonate at different frequencies given the same binding environment. By "tuning" into the appropriate frequency range, it would be possible to selectively visualize microcalcifications of varying sizes

Body:

At the writing of this report, we are currently 21.5 months into our project. Dr. Weinstein coordinated the project with Dr. Seghal. Dr. Weinstein has been involved in patient selection and in performing the imaging evaluation along with the research coordinator. Dr. Seghal has organized the imaging protocol and is overseeing the digitizing of the images and data analysis performed in the Ultrasound Research Laboratory.

Task 1: See report from 7/1/00-6/30-02.

Task 2: Patient recruitment period completed

Task 3: Ongoing patient recruitment. Continuation of Task 2.

Since the writing of out last report, we have been involved in patient accrual for the study. To this date, we have accrued thirty- two patients. In thirty-one of those patients, data was obtained for the study. Due to technical factors, data could not be obtained from one of the patients. We have made significant progress in patient recruitment since the writing of our last annual report. Although we are slightly behind schedule, we are optimistic that we will continue to accrue at the current pace.

The patients present to the Breast Imaging Section of the Hospital of the University of Pennsylvania on the day of their biopsy procedure. The patients recruited for the study have breast microcalcifications that are considered suspicious. The patients may undergo excisional biopsy in the operating suite by a surgeon. Alternatively, they may undergo percutaneous core needle biopsy in the Breast Imaging Section in order to obtain a tissue diagnosis. Prior to either of these conventional biopsy procedures the patients are recruited for the study.

The age of the patients have ranged from 40 to 83 years. The breakdown of the age of the patient population is shown in Figure 1 by the decade. The demographics of the patient population is shown in Figure 2. Thus far, out of the 31 patients, 20 patients had benign calcifications on pathologic evaluation and 11 patients had calcifications that were demonstrated to be malignant (Figure 3). Figure 4 shows the age of the patients relative to the pathology results.

First gray scale imaging was performed at the site of the microcalcifications. Next, the same area was scanned in Power Doppler mode in conjunction with acoustic resonance. The acoustic resonance device emitted low frequency vibrations in 10 Hz steps between 50-600 Hz. In the first nine patients, 100 Hz steps were utilized, and it was decided that the steps too large and a decision was made to utilize smaller incremental steps. The scanning was repeated using 3 different vibration amplitudes to determine variation and the frequency of response of the calcifications to the variation in the amplitude. All the images were stored on a videotape and used for quantitative analysis.

The mammogram from each patient was digitized at 300 DPI and stored in the database for future review. The ultrasound examination was performed using state of the

art ATL 5000 ultrasound scanner. All imaging was performed with 12.5 MHz broadband transducer. The instrument resets determined from the studies conducted in the first year were used for all patients.

The acoustic resonance scans involving low frequency vibrations were tolerated by all the patients. We have had no adverse reactions to date. Average total of scan time was approximately 15 minutes. Imaging was completed successfully in 31/32 patients. In 1 case, the examination was not completed due to problems with the scanning equipment.

We have completed quantitative analysis of images from all of the patients enrolled in the study to date. This involved digitizing the images from the videotape. The images of each patients were compiled in a single file and used for quantitative measurement of mean mean color level (MCL), percent area of color (FA) and color weighted fractional area (CWFA). The analysis was performed by selecting the entire image as proposed in the application. However, the results show that structures other than calcifications, such as connective tissue are also enhanced by the acoustic resonance imaging. In view of these results we believe that the images may have to be re-analyzed by choosing specific area of interest to decrease the background noise.

Of the 31 patients studied, 20 cases (64.5 %) were benign and the remaining 11 cases (35.5 %) were malignant. Figure 5 shows an example of images obtained from a patient with malignant calcifications. The mammogram in 5a shows a cluster of calcifications. The biopsy proven malignant calcifications are circled. Figures 5b-d show 3 representative ultrasound images at 50 Hz, 350 Hz and 480 Hz from a total of 165 images. In the gray scale image Figure 5b (50 Hz), calcifications cannot be seen with any

level of confidence. As the frequency of vibration increases, at 350 Hz, calcifications can be seen in color superimposed on gray scale image. At 350 Hz (Figure 5c), the power Doppler pixels, representing calcifications, are in a distribution pattern that is very similar to that seen on the mammogram Figure 5a. In addition to the calcifications, enhancement of secondary structures associated with ducts and connective tissue are also observed (arrow) in Figure 5c. At higher frequency, this effect becomes significant and can mask the calcifications. This is shown in Figure 5 d imaged at 480 Hz. The inset panel (Figure 5e) showing a graph represents change in image enhancement (CWFA) as a function of vibration frequency (Hz). The error bars on the data point represent +/- image deviation of the three measurements at three different scanning parameters. On all three different scans, the graph demonstrates a clear resonance peak at 480 Hz.

Figure 6 shows the results from a patient with benign calcifications. Figure 6a shows the mammographic image of the calcifications. There is a focal cluster of calcifications that is circled. Figure 6b demonstrates the region of the calcifications in gray scale. Again, the calcifications are difficult to discern. However, there is enhancement seen at 280 Hz. The expected region of calcifications is circled. However, there is significant enhancement of secondary structures present. Conclusions are similar to those obtained from Figure 5.

The peak position (P) and the width of the peak at half height (W) were measured for each patient. These values are summarized in Table 1. In all patients with malignant calcifications, enhancement was seen in the power Doppler mode and a peak in CWFA vs. frequency curve was observed in all the cases. The mean +/- standard deviation for the peak position (P) was 363 +/- 132. The peak width (W) was 132 +/- 50 Hz. In

patients with benign calcifications, the image enhancement was observed in 18 (90%) of 20 cases studied. Two cases did not show any measurable enhancement. The mean +/- standard deviation for the peak position and peak width were 381 +/- 111 Hz and 122 +/- 54 Hz respectively. There appears to be no significant difference in the peak width and peak position between the benign and malignant calcifications.

Technical Issues:

In the last annual report review, a technical issue was raised. The size of the particles used in the phantoms was questioned. The particle size used in the phantom work ranged from 400-800μ. While some malignant breast microcalcifications may be smaller than this size, benign breast calcifications may vary greatly in size and certainly fall within this size range.

Once we are able to recruit a pathologist for the study. The actual size of the particles will be measured from the pathologic specimen.

Key Research Accomplishments:

- We have been able to visualize calcifications with power Doppler and acoustic resonance in patient studies in 29/31 patients. No significant enhancement could be seen in two patients who both had benign calcifications.
- The visualized calcifications demonstrated a resonance peak.

- There was no significant difference in the resonance peaks between the malignant and benign calcifications

Reportable Outcomes:

Weinstein SP, Conant EF, Patton J, Seghal CM. Targeting and core biopsy of breast microcalcifications under ultrasound using acoustic resonance. Radiological Society of North America 1999. (see appendices)

Weinstein SP, Seghal C, Conant EF, Patton JA. Microcalcifications in Breast tissue Phantoms Visualized with Acoustic Resonance Coupled with Power Doppler US: Initial Observations. Radiology 2002;224:265-269. (see appendices)

Conclusions:

The results of this study to date show that while we were able to observe calcifications using power Doppler and acoustic resonance in the majority of the cases (29/31), there is no significant difference could be observed between the malignant and the benign calcifications. At this stage of the study, we speculate, that the lack of differentiation between the two types may be associated with the enhancement from the secondary structure such as ducts and connective tissues of the breast that would be seen with both benign and malignant calcifications.

At present analysis, we have analyzed the entire region present in the image field of view. This includes the enhancement of secondary structures. To overcome this limitation, the image data must be re-analyzed. We propose to review the images and select out the regions that represents connective tissues. These areas and the image will be discarded from the analysis to determine if the enhancement of calcifications did mask in the differentiation between the malignant and benign calcifications.

References:

Soderstrom CE, Harms SE, Copit DS, et al. Three-dimensional RODEO breast MR imaging of lesions containing ductal carcinoma in situ. Radiology 1996; 201:427-432.

Orel SG, Medonica MH, Reynolds C, et al. MR imaging of ductal carcinoma in situ. Radiology 1997;202:413-420.

Gilles R, Zafrani B, Guinebretiere JM, et al. Ductal carcinoma in situ: MR imaging-histopathologic correlation. Radiology 1995;196:415-419.

Kopans D. Pathologic, Mammographic, and Sonographic Correlation. In: Kopans, Daniel, ed. Breast Imaging. 2nd ed. Philadelphia: Lippincott-Raven, 1998; 511-615.

Ernster VL, Barclay J, Kerlikowske K, Wilkie H, Ballard-Barbash R. Mortality among women with ductal carcinoma in situ of the breast in the population-based surveillance, epidemiology and end results program. Arch Intern Med 2000;160:953-958.

Appendices:

See attatched

Figure 1

Age of the Patients

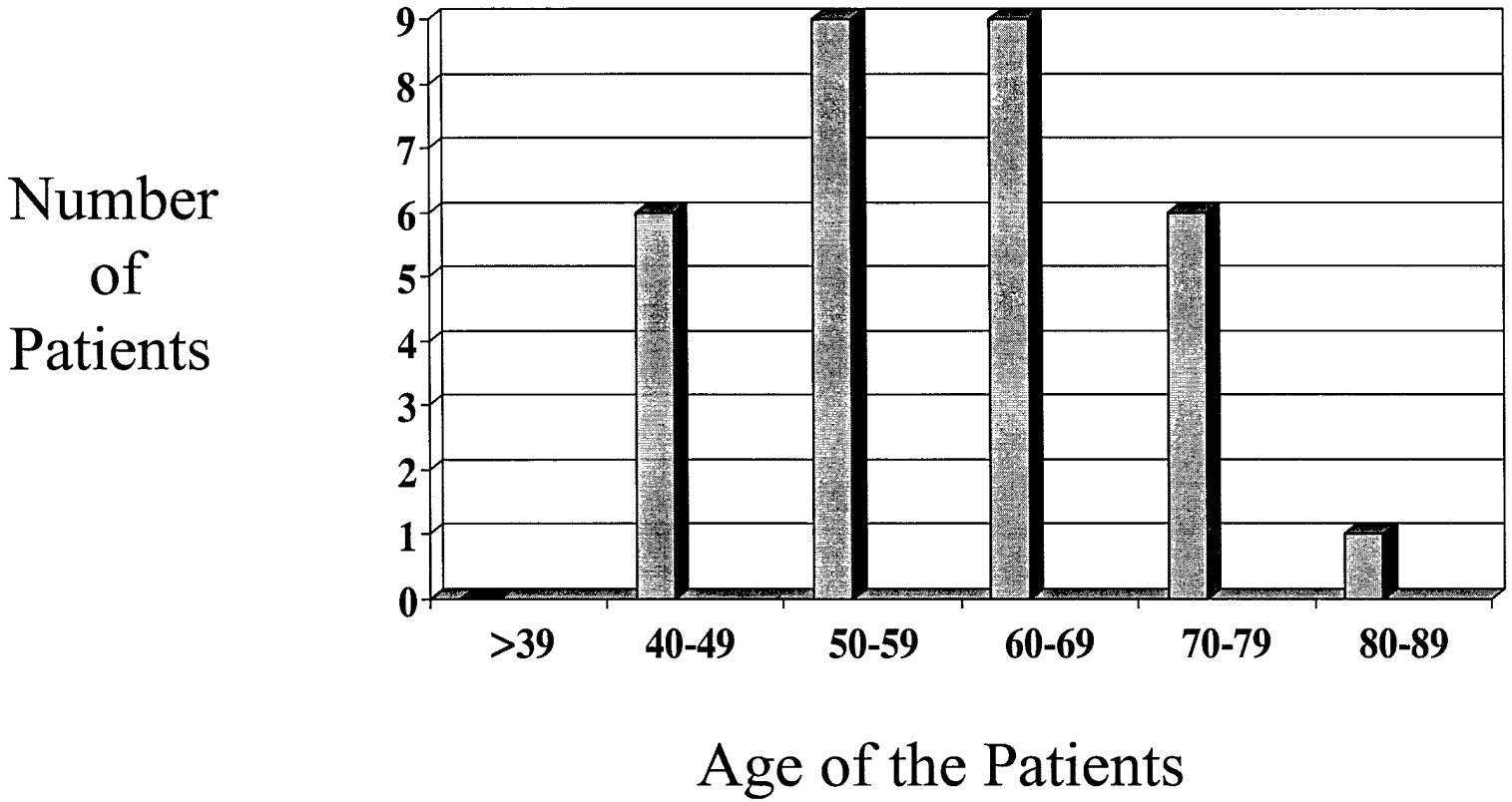

Figure 2

Benign Vs. Malignant Calcifications

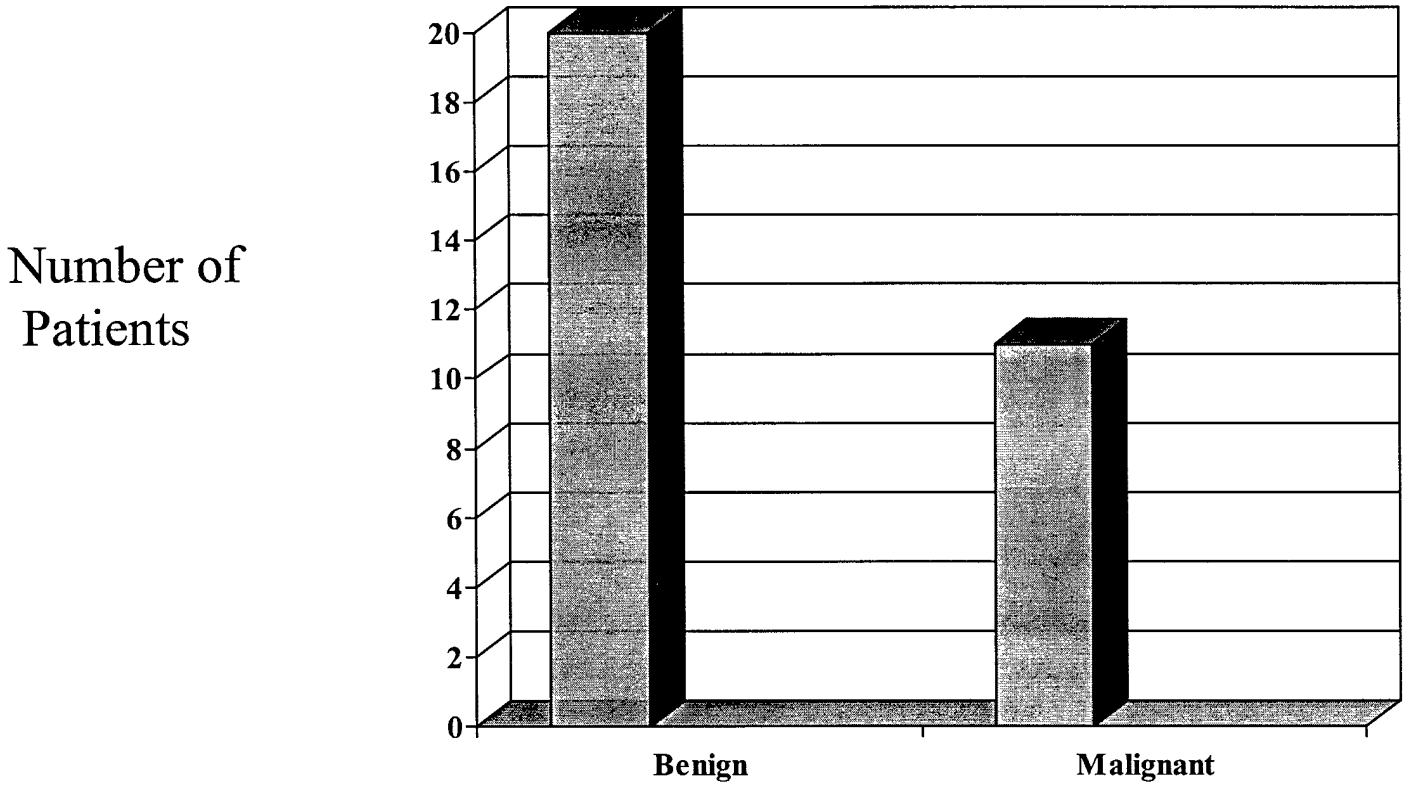

Figure 3

Age of the Patients vs. Pathology

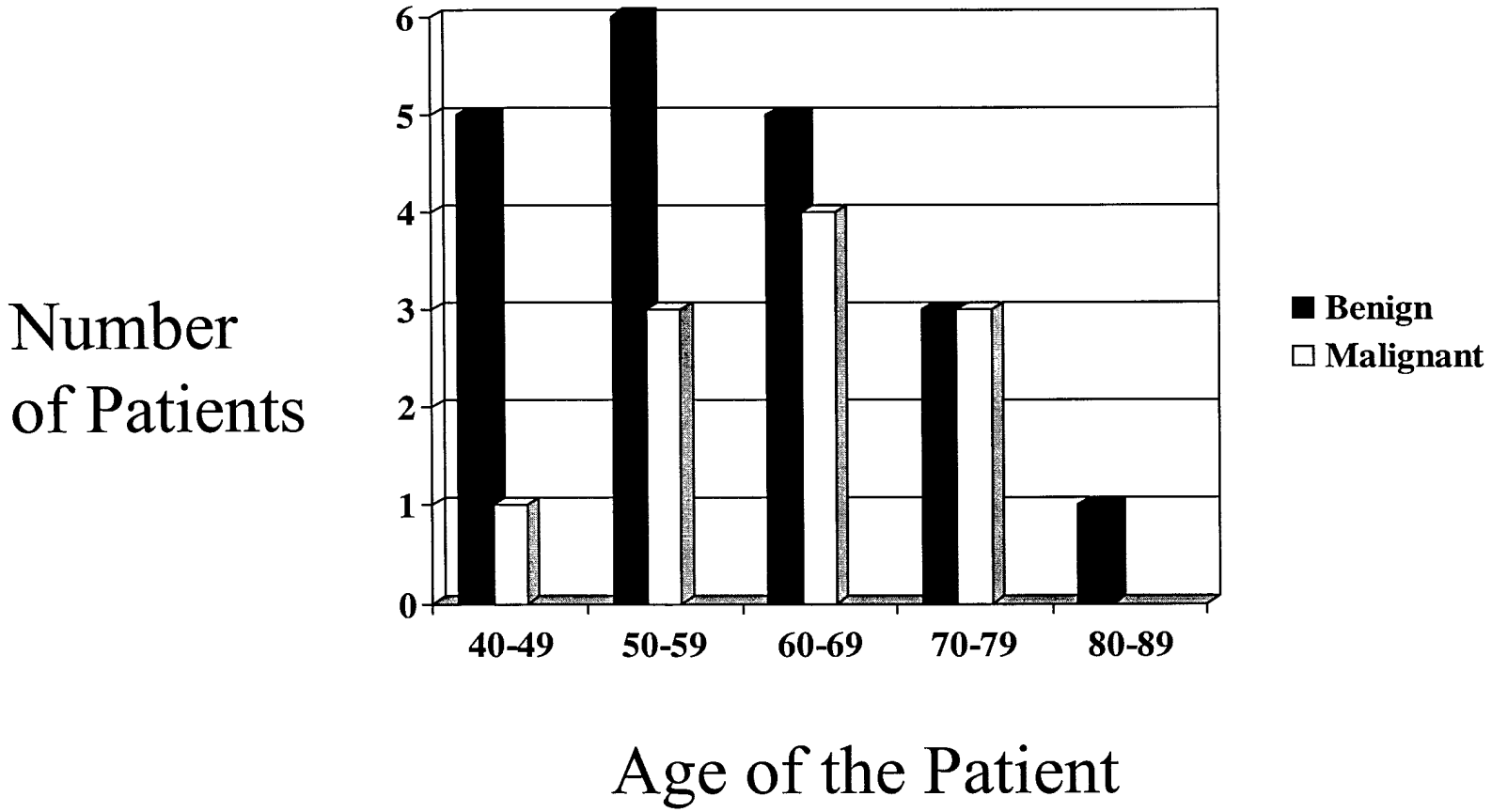

Figure 4

Demographics

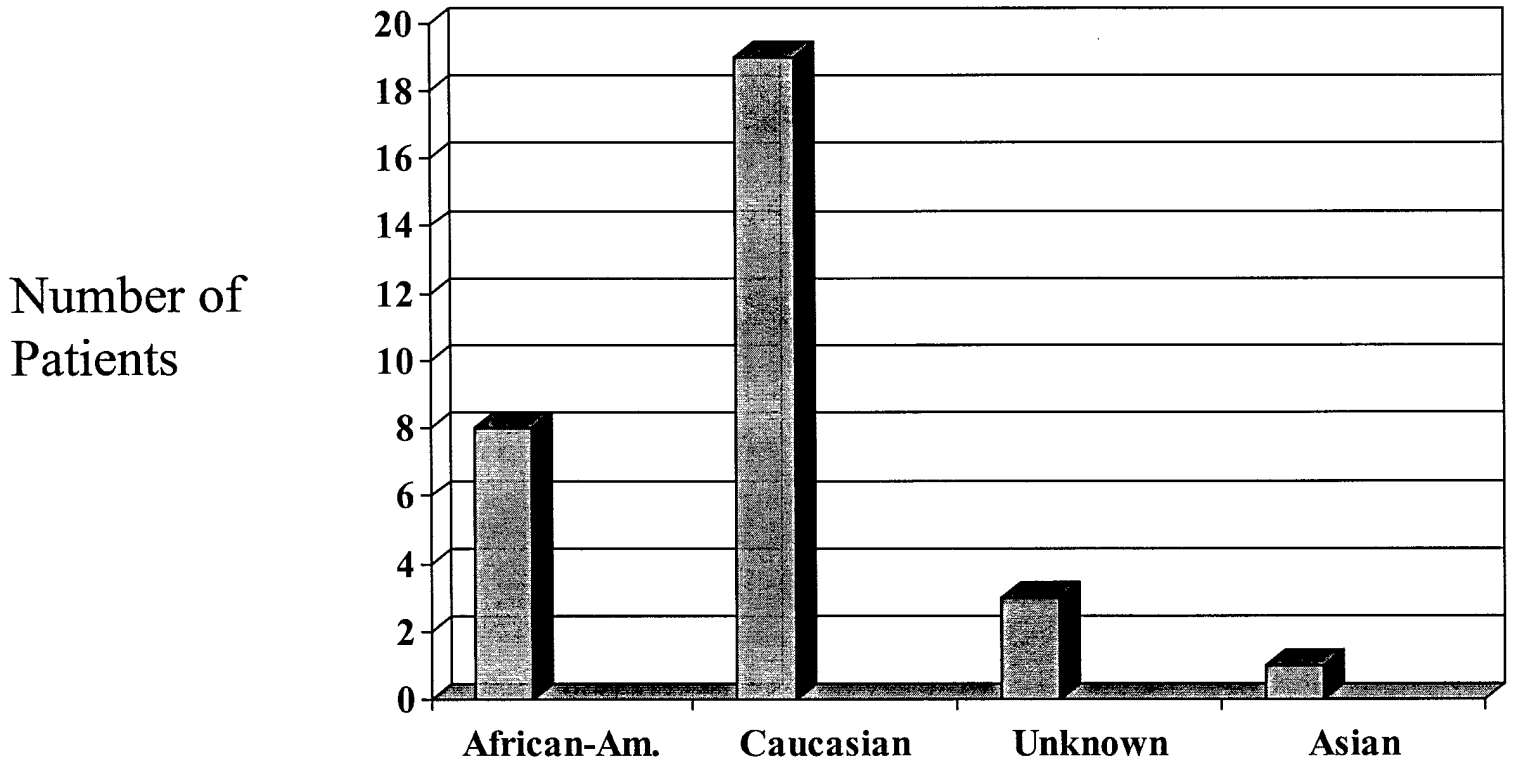

Fig. 5

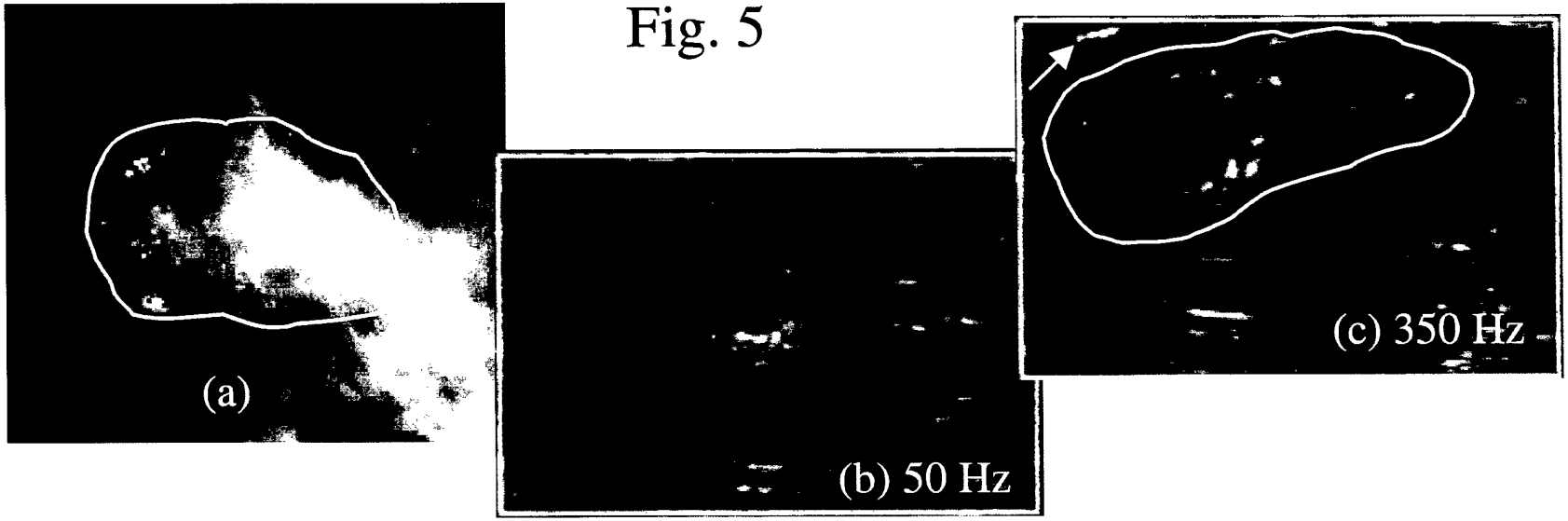
(a)
(b) 50 Hz
(c) 350 Hz

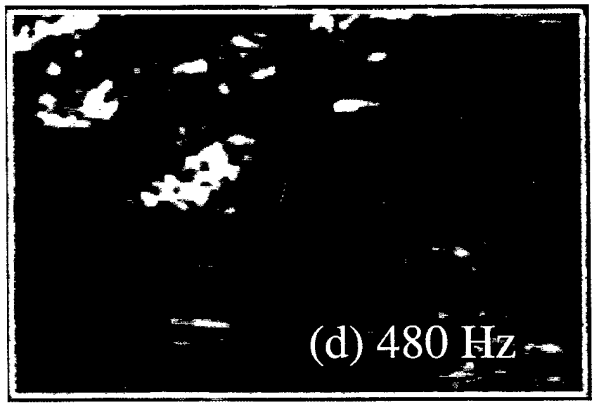
(d) 480 Hz

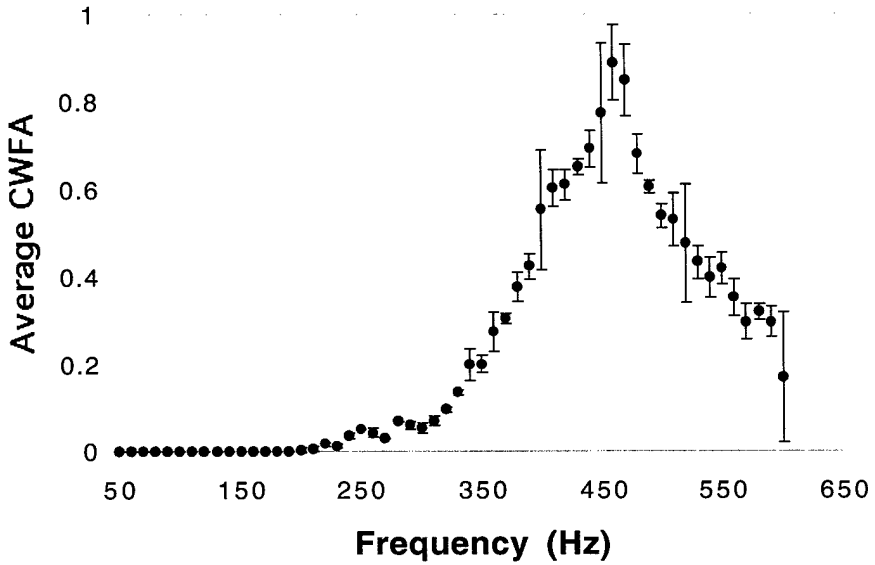
Average CWFA
1
0.8
0.6
0.4
0.2
0
50
150
250
350
450
550
650
Frequency (Hz)

(e)

Fig. 6

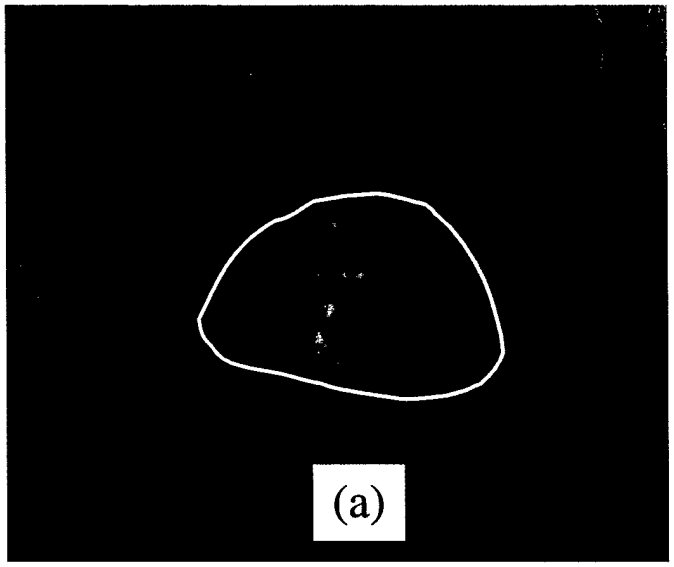
(a)

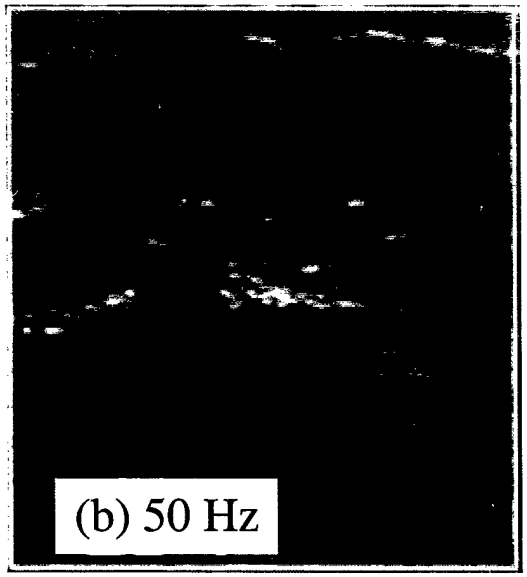
(b) 50 Hz

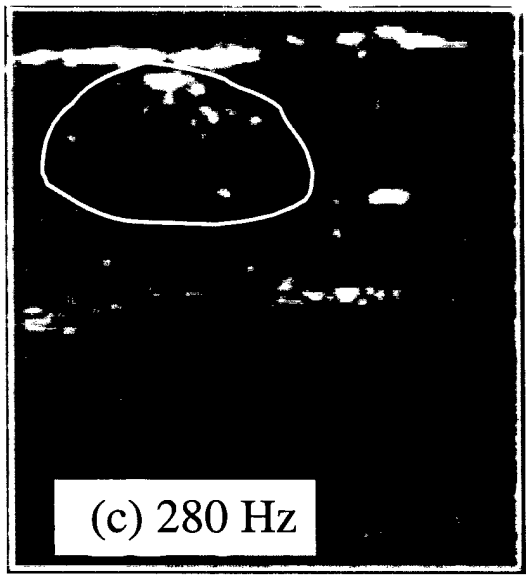
(c) 280 Hz

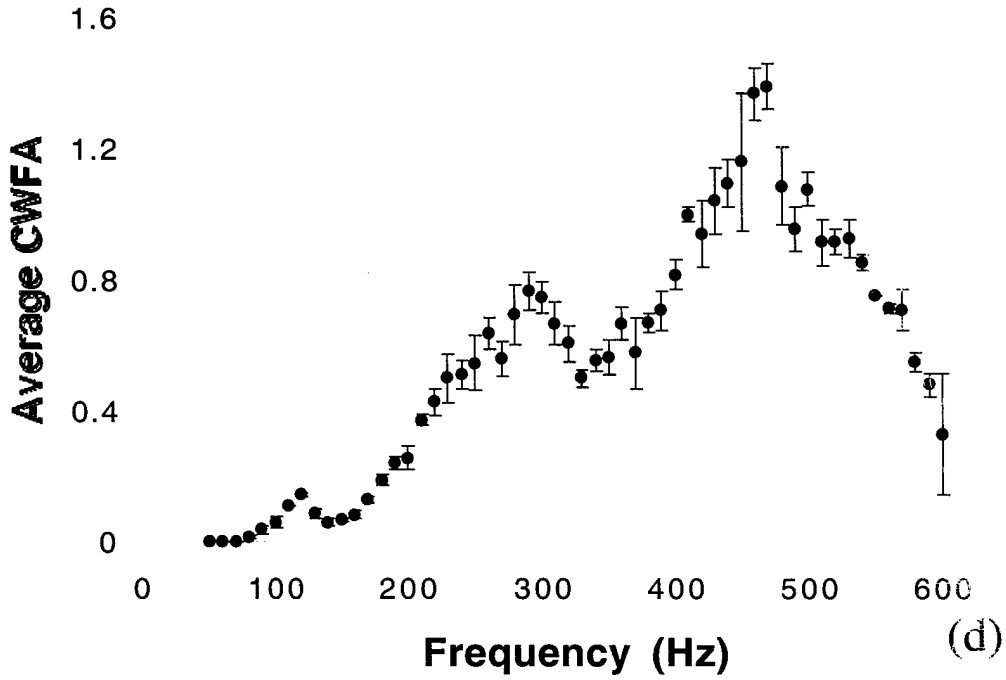
1.6
1.2
0.8
0.4
0
Average CWFA
0
100
200
300
400
500
600
Frequency (Hz)
(d)

Table 1.

Patient #	Benign		Malignant	
	Peak Position	Peak Width	Peak Position	Peak Width
	P (Hz)	W (Hz)	P (Hz)	W (Hz)
1	477	120	460	158
2	184	69	500	100
3	250	27	400	100
4	526	150	285	99
5	428	217	100	100
6	560	75	191	56
7	400	245	277	120
8	154	63	450	120
9	280	120	425	203
10	318	116	400	200
11	383	119	500	200
12	342	122		
13	464	116		
14	467	178		
15	460	142		
16	363	153		
17	395	85		
18	411	82		
19	No enhancement			
20	No enhancement			
Mean	381	122	363	132
St. dev.	111	54	132	50

Figure Legends:

Figure 1.
Figure 1 demonstrates the age distribution of the patients who participated in the study.

Figure 2.
Figure 2 shows the number of benign and malignant calcifications that have thus far been imaged and evaluated.

Figure 3.
Figure 3 show the age distribution of the patients and the number of benign and malignant calcifications in each of the age groups.

Figure 4.
Figure 4 shows the demographics of the patients who participated in the study.

Figure 5.

A. A mammographic image of the malignant calcifications is demonstrated. The calcifications are circled.
B. A sonographic image of the region of the calcifications is shown. The calcifications are difficult to see at 50 Hz.
C. At 350 Hz, there are power Doppler pixels demonstrated. The expected region of the calcifications is circled.
D. At 480 Hz, there is increased enhancement of the secondary structures.
E. The graph shows the degree of enhancement as a function of frequency. There is a clear resonance peak at 480 Hz.

Figure 6.

A. A mammographic image from a patient with biopsy proven benign calcifications is shown. The calcifications are circled.

B-C. No significant enhancement is seen at 50 Hz. At 280 Hz, enhancement in the region of the calcifications (circled) is seen but there is also enhancement of the surrounding secondary structures in the breast.

D. The graph of degree enhancement vs. frequency again shows a resonance peak at approximately at 480 Hz, similar to the value seen with malignant calcifications.

Table 1.
Table 1 shows the peak position (P) and the width of the peak at half height (W) for malignant and benign calcifications. There appears to be no significant difference between these two values for malignant and benign calcifications.

...opy images were concealed and the film panels were numbered and ...only labeled as A or B to identify the tissue harmonic and conven... formats. Three radiologists interpreted the images blindly and ...endently in two separate reading sessions. First, a side-by-side ...parison of image quality was performed. Lesion conspicuity, presence ...ernal echoes, extent of through transmission and wall definition were ...as A definitely better than B, A probably better, no difference, B ...ably better, and B definitely better. In a second blinded reading ...on, each mass was independently characterized as cystic or solid. All ...lesions were confirmed pathologically and all cysts were confirmed ...ecific aspiration and subsequent collapse of the lesion.
RESULTS: There were 37 solid lesions and 27 cysts. For all three readers, ...e harmonic imaging was rated as better for each category of image ...ar significantly more often than conventional sonography. For cysts: 9 ...ons read as solid and 5 lesions read as indeterminate on conventional ...graphy were correctly classified as cysts on harmonic imaging. Only ...cysts were incorrectly classified as solid on harmonic imaging and ...ectly classified as cysts on conventional imaging. For solid lesions: 2 ...sified as cysts and 5 classified as indeterminate on conventional ...graphy were correctly classified as solid on harmonic imaging. Two ...ions read as cysts and one lesion read as indeterminate on harmonic ...aging were correctly classified as solid on conventional imaging. No ...ion read as definitely a cyst on harmonic imaging turned out to be solid.
CONCLUSIONS: These preliminary results suggest that tissue harmonic ...aging improves the quality and visualization of breast masses and may ...ovide more accurate characterization of breast cysts.

1177 • 2:39 PM
...npalpable Breast Lesions: Evaluation with Power Doppler US and a ...icrobubble Contrast Agent

...K. Moon, MD, Seoul, South Korea • J. Im, MD • D. Noh, MD • K.M. Yeon, MD • ...C. Han, MD

...URPOSE: To evaluate the value of power Doppler (PD) US and a ...icrobubble US contrast agent in differentiation of nonpalpable breast ...sions.
METHOD AND MATERIALS: Fifty patients (age range, 32-65 years; ...edian age, 53 years) with nonpalpable breast lesions detected on ...ammograms and visualized by gray-scale US with 10 MHz transducer ...ere prospectively evaluated with PDUS before and after injection of the ...ontrast agent SHU 508A at a concentration of 400 mg/ml. In 12 patients ...ith multiple lesions, the most suspicious lesion was targeted. Surgical ...cision of 30 nonpalpable lesions after needle localization revealed 8 ...nfiltrating and 14 intraductal carcinomas and 28 benign diseases. Mean ...esion size was 11 mm and 10 mm in each group. Lesion vascularity ...avascular, hypovascular, hypervascular), distribution (central vs periph...eral) and morphology (regular vs irregular) of vessels were analyzed by ...wo radiologists subjectively and correlated with mammographic charac...teristics and histopathologic results.
RESULTS: At unenhanced PDUS, 8/22 (36%) cancers were vascular (5 ...ypovascular and 3 hypervascular) whereas 4/28 (14%) benign lesions ...ere vascular (3 hypovascular and 1 hypervascular). After injection of ...ontrast agent, 21/22 (95%) cancers were vascular (8 hypovascular and 13 ...ypervascular) whereas 6/28 (21%) benign lesions were vascular (4 ...ypovascular and 2 hypervascular). 18/22 (82%) cancers and 3/28 (11%) ...enign lesions showed an increase in vascularity by the contrast agent. In ...ancers, distribution of vessels was 3 peripheral, 1 central and 4 both at ...unenhanced PDUS and 4 peripheral, 4 central and 13 both at contrast-...nhanced PDUS. In benign lesions, it was 3 peripheral and 1 both at ...unenhanced PDUS and 4 peripheral, 1 central and 1 both at contrast-...nhanced PDUS. Irregular vessels were seen in 3/8 (38%) malignant and ...1/4 (25%) benign lesions at unenhanced PDUS and 11/21 (52%) malignant ...and 2/6 (33%) benign lesions at contrast-enhanced PDUS. After injection of ...contrast agent, 6/8 infiltrating cancers were hypervascular whereas 7/14 ...ntraductal cancers were hypervascular. Characteristics of benign lesions ...with the vascularity were subareolar (4/6) in location, nodular density ...without microcalcifications at mammography (5/6) and fibrocystic disease ...or papilloma at pathologic examination (6/6).
CONCLUSIONS: At PDUS of nonpalpable breast lesions, an increase in ...vascularity by contrast agent was predominantly seen in malignant lesions. ...Contrast-enhanced PDUS may be helpful for the differentiation of nonpal...pable breast lesions.

1178 • 2:48 PM
High Rate of Sonographic Detection of DCIS Calcification in Mammographically-directed High Frequency Ultrasound Breast Exams

B.E. Hashimoto, MD, Seattle, WA • L. Wiitala, BA • V. Picozzi, MD • D.J. Kramer, MD • M.E. Lee, MD • S.M. Boswell, MD

PURPOSE: To assess the high frequency ultrasound characteristics of pure ductal carcinoma in situ (DCIS) of the breast.
METHOD AND MATERIALS: We retrospectively reviewed all cases of breast DCIS sonographically evaluated at our institution during the last 2 years. Patients were excluded if pathologic (lumpectomy or mastectomy) specimens contained invasive carcinoma in addition to DCIS. We used commercially available ultrasound equipment (Acuson, Mountain View, CA) with a high frequency transducer (8-13MHz). Cases were analyzed for (1)histologic grade, (2)mammographic findings, and (3)ultrasound findings.
RESULTS: 18 patients met the above criteria. All patients presented with mammographic clustered pleomorphic calcifications. These calcifications were sonographically identified in 17(94%). Sonographically, these calcifications were within focally dilated ducts 3/18(13%), in normal breast tissue 6/18(33%) or within a mass 3/18(44%). These patients had the following DCIS histologic grades: 11(61%) high, 4(22%) intermediate, 2(11%) low. Calcifications with mass or dilated ducts represented 9/11(82%) high grade and only 2/6(33%) intermediate or low grade neoplasms. This difference is statistically significant ($p<0.005$). Sonographic analysis of the 5 masses demonstrated the following characteristics. Mean mass size was 12 mm. All masses had ill defined margins. Shape was irregular in 3, oval in 2. The masses had the following echogenicity: 3 hypoechoic, 2 heterogeneous. Six masses shadowed (2 had edge shadowing, 2 shadowed distal to mass, 2 had shadows obscuring the mass). Four masses were associated with architectural distortion and spiculation.
CONCLUSIONS: High resolution ultrasound can detect a high rate (94%) of DCIS calcifications and is frequently (65%) associated with other sonographic abnormalities (dilated ducts or mass). Furthermore, high grade DCIS was much more likely to display these additional abnormalities than nonhigh grade DCIS ($p<0.005$). Further investigation is needed to explore whether these sonographic findings may add to mammographic prediction of breast malignancy or provide information to direct sonographic biopsy guidance for patients who cannot tolerate mammographic biopsy positioning. (BEH, DJK, and SMB test equipment for Acuson Corp, Mountain View, CA)

1179 • 2:57 PM
The Specificity of Combined Mammographic and Ultrasonographic Evaluation of Palpable Lumps and Palpable Thickening

D.B. Kopans, MD, Boston, MA • R.H. Moore, AB • P.J. Slanetz, MD, MPH • E.D. Yeh, MD • D.A. Hall, MD • K.A. McCarthy, MD

PURPOSE: To determine the likelihood of breast cancer when both the mammogram and ultrasound show normal appearing breast tissue in women referred with a clinically palpable lump or thickening.
METHOD AND MATERIALS: The computerized records of the Breast Imaging Division of the Massachusetts General Hopsital were reviewed to determine the number of women evaluated between 1/1/95 and 12/31/98; the number of these who were referred for evaluation of a palpable lump or thickening; the number of these who had a normal mammogram and ultrasound, the number of these who had a breast biopsy and the number of these who proved to have cancer.
RESULTS: 37,301 women were evaluated. 3328 had been referred for a palpable lump or thickening. 430 had normal appearing mammograms and ultrasound studies. 67 of these had breast biopsies. 1 cancer was diagnosed.
CONCLUSIONS: If the mammogram and ultrasound show completely normal breast tissue, the likelihood of a palpable finding being malignant is extremely low.

1180 • 3:06 PM
Targeting and Core Biopsy of Breast Microcalcifications under Ultrasound Using Acoustic Resonance

S.P. Weinstein, MD, Philadelphia, PA • E.F. Conant, MD • J. Patton, BS, MS • C.M. Sehgal, PhD

PURPOSE: We have developed a novel method by which calcium particles can be brought to acoustic resonance and visualized with the aid of power Doppler ultrasound. The goal of this study is to demonstrate that breast microcalcifications detected with this method can be core biopsied under its guidance in gelatin phantom and tissue models.
METHOD AND MATERIALS: Our previous studies have demonstrated that breast microcalcifications may be detected by acoustic resonance imaging. Gelatin phantoms were made with calcium carbonate particles (≈400-800m). The particles were evaluated with power Doppler imaging while resonating the particles at 50-500 Hz. At maximum color visibility the particles were targeted and biopsied using a 14g core needle. The phantom and core samples were x-rayed to demonstrate that the area of color detection represented the calcium particles. The images were videotaped and analyzed quantitatively for mean color level (MCL), % area of color (FA) and color weighted fractional area (WFA). The experiments were repeated using turkey phantom models with embedded calcium particles.
RESULTS: The plot of MCL, FA, WFA vs. frequency peaked and fell in a bell shaped curve reaching maximum at ≈200–300 Hz. At this frequency, optimal visualization of the particles was observed and enabled localization and biopsy of the microcalcifications under ultrasound guidance.

CONCLUSIONS: Data using phantoms demonstrated that microcalcifications may be targeted under ultrasound with power Doppler and acoustic resonance allowing for dynamic ultrasound guided core biopsy.

1181 • 3:15 PM

Echogenic Breast Carcinomas

L.A. Hardesty, MD, Pittsburgh, PA • K.M. Harms, MD

PURPOSE: Prior studies, including Stavros et al's landmark article (Radiology 1995), have suggested that intense and uniform hyperechogenicity allow a breast mass to be classified as benign and avoid biopsy. Contrary to this, we describe the features of a series of echogenic breast carcinomas.
METHOD AND MATERIALS: Between 1/90 - 10/96, one of the authors (KH) collected a series of ten echogenic breast cancers from her daily practice. The following features of these were retrospectively reviewed: margin (ill- or well-defined), palpability, shape (oval, round, irregular, lobulated), echotexture (homogeneous, heterogeneous), sound transmission (enhance, shadow, neither), and whether the lesion was "taller-than-wide" (AP dimension greater than transverse or sagittal dimension) or "wider-than-tall". All lesions underwent surgical excision and were proven to be carcinomas.
RESULTS: There were nine cases of infiltrating ductal carcinoma and one case of ductal carcinoma in situ. All lesions had ill-defined margins. 8/10 lesions were palpable, 8/10 had an irregular shape, and 9/10 were homogeneously hyperechoic. 4/10 lesions caused posterior acoustic shadowing while 6/10 lesions had neither posterior acoustic shadowing nor enhancement. 1/10 lesions was "taller-than-wide" while 5/10 lesions were "wider-than-tall" and 4/10 lesions were of approximately equal height and width.
CONCLUSIONS: Although the great majority of uniformly hyperechoic breast masses are benign, breast imagers must remain aware that there are exceptions, and that hyperechoic breast cancers, though rare, exist. Features associated with hyperechoic cancers were ill-defined margins, irregular shape and being palpable.

Wednesday Afternoon • Room S403B

■ Radiation Oncology (Sarcoma, Biology)

PRESIDING: Lewis G. Smith III, MD, Houston, TX
Computer Code: P06 • 1½ hours
To receive credit, relinquish attendance voucher at end of session.

1182 • 2:30 PM

Image Fusion: A New Approach for Using MR Imaging in Brachytherapy

R.C. Krempien, MD, Heidelberg, Germany • W. Harms, MD • H.A. Grabowski, PhD • F.W. Hensley, PhD • M. Treiber, MD • M. Wannenmacher, MD, DDS

PURPOSE: _Accurate definition of tumor volume is essential for brachytherapy treatment planing. CT accurately localize sources, but often poorly delineates tumor. MRI has several imaging benefits such as improved soft tissue definition and unrestricted multiplanar imaging but does not visualize the source dwell positions. The aim of this study was to access the possibilities of a new developed system generating synthetic image modalities from matched and fused CT and MRI-data in brachytherapy planing.
METHOD AND MATERIALS: _The system presented consists of five modules serving for viewing, matching, segmentation, fusion and validation. The automatic registration takes about one minute for two data sets of about 60 slices. Depending on slice thickness the registration algorithm is able to register MRI and CT data in over 95% of the cases without any interaction with an average accuracy of the calculated transformation bellow 1mm. The segmentation module consists of two modes, the volume mode for three dimensional region growing to segment connected structures and the slice mode for interactive slice by slice segmentation of the superimposed previously registered images. Tumor structures or source dwell positions can be segmented in any plane in one imaging modality and then copied into the other. Reconstruction of the fused images in different planes offer the possibility to validate the matching accuracy.
RESULTS: _A patient with liposarcoma in the thigh showed a positive tumor margin to the ischiadic nerve. Intraoperativley the decision was made to implant brachytherapy guides for postoperative boost-radiation of the tumor-bed rather than resecting the nerve to preserve the function of the leg. CT accurately localizes source positions but the nerve as the primary target structure was hardly detectable. The MRI visualized the nerve but the source positions could not be detected. The ischiadic nerve was segmented in MRI and the gray values of the segmented structure were copied in the CT image. The source positions are segmented via seed points in the CT. The Position of the nerve can now be visualized in comparison to the source dwell positions. The synthetic images are added into the brachytherapy planing system. The CT-based brachytherapy-planing would have resulted in a miscalculation of the target volume while the synthetic images lead to a optimization in therapy planing.
CONCLUSIONS: _These preliminary data show that image registration and fusion is feasible for brachytherapy planing. In the shown case the use of synthetic images in brachytherapy planing lead to a optimized treatment planing.

1183 • 2:39 PM

Invited Presentation from ASTRO: Morbidity and Long-term Results of Adjuvant Brachytherapy in Soft Tissue Sarcoma: A Prospective Randomized Trial

K. Alektiar, MD, New York, NY

PURPOSE: We have previously shown that adjuvant brachytherapy (BRT) improves local control in soft tissue sarcoma (STS) of the extremity and superficial trunk (JCO 14:859–868, 1996). The morbidity of such an approach however, has not been examined. The purpose of this study was to evaluate the toxicity associated with adjuvant BRT and to extend our observations through eight years of median follow-up.
MATERIALS AND METHODS: Between 7/82 and 6/92, 164 adult patients with STS of the extremity or superficial trunk were randomized intraoperatively to receive or not to receive BRT after complete resection. BRT was delivered with Ir-192 to a total dose of 42–45 Gy. The BRT and no BRT groups were balanced with regard to age, sex, presentation (primary vs recurrent), site, grade, size, and depth. Morbidity was assessed in terms of significant wound complication, bone fracture, and peripheral nerve damage (grade ≥3). Significant wound complication was defined as wound infection or complication requiring further operative intervention. The median follow-up was 8 years.
RESULTS: The significant wound complication rate was 24% in the BRT group and 15% in the no BRT group, $p = 0.18$. The rate of wound re-operation, however, was significantly higher in the BRT arm (9% vs. 1%, $p = 0.03$). Examination of other co-variables that may have contributed to wound re-operation, revealed the width of the excised skin (WES) to be a significant factor [1% (WES ≤ 4 cm), vs. 10% (WES 4 cm), $p = 0.02$]. The rates of bone fracture and nerve damage were higher in the BRT arm but the differences did not reach statistical significance [5% vs. 0% ($p = 0.18$) and 9% vs. 3% ($p = 0.3$), respectively]. At 8 years, the actuarial local control rate was 81% in the BRT arm vs. 64% in the no BRT arm ($p = 0.03$). The local control for high grade tumors was 89% in the BRT group compared to 62% in the no BRT group ($p = 0.001$). BRT had no impact on local control in patients with low grade tumors ($p = 0.4$) and no impact on overall survival ($p = .18$) or disease-free survival ($p = 0.3$).
CONCLUSION: Based on this update, adjuvant brachytherapy continues to show improvement in local control for high grade STS of the extremity and superficial trunk, but no improvement in overall or disease- free survival. The overall morbidity associated with adjuvant BRT was not significantly higher than that with surgery alone. However, BRT and WES 4 cm, were associated with significantly higher wound re-operation rate. This has significant implications for strategies designed to maximize wound coverage in patients who receive BRT.

1184 • 2:48 PM

MRI May Be Used to Evaluate the Effects of Tumor Oxygenating Agents on Radiosensitivity

H.A. Al-Hallaq, AB, Chicago, IL • M.A. Zamora, BS • B.L. Fisn, BS • J.E. Moulder, PhD • G.S. Karczmar, PhD

PURPOSE: Previous work suggested that MRI could provide noninvasive, high resolution measurements of the effects of tumor oxygenating treatments (TOX's) on tumor blood and tissue oxygen levels. Here we evaluate whether MRI can be used to rank TOX's according to their effectiveness in increasing tumor response to radiation.
METHOD AND MATERIALS: Studies of BA1112 rhabdomyosarcomas in WAG/rij rats have shown that infusion of a perfluorocarbon emulsion (PFC) combined with carbogen (95% O_2/5% CO_2) breathing significantly increased radiosensitivity relative to either treatment alone. We investigated whether MRI correctly predicts the relative efficacy of treatment with carbogen or PFC alone compared to treatment with PFC + carbogen in this tumor model. We used MR signal linewidth, i.e., blood-oxygen-level-dependent (BOLD) contrast, as an index of change in tissue oxygen tension. Decreases in linewidth indicate increases in tumor oxygenation. To assess the spatial distribution of response, maps of pixels that responded to treatment were generated for each tumor.
RESULTS: Average MR signal linewidth decreased by 2.7% during carbogen breathing, by 2.3% during PFC + air, and by 6.3% during PFC + carbogen (n=7). The change caused by PFC + carbogen was significantly greater than the change caused by either treatment alone ($p < 0.01$ by paired t-test) demonstrating that the combined treatment increases tumor oxygenation more than PFC or carbogen alone. Percentages of responding pixels in each category were averaged over all 7 tumors. 22% of tumor pixels responded to treatment with carbogen while 32% of pixels re-

Susan P. Weinstein, MD
Chandra Seghal, PhD
Emily F. Conant, MD
Jill A. Patton, MS

Index terms:
Breast, calcification, 00.8119
Breast, US, 00.12981
Breast radiography, technology, 00.128

Published online before print
10.1148/radiol.2241010511
Radiology 2002; 224:265–269

[1] From the Department of Radiology, University of Pennsylvania Medical Center, 1 Silverstein Bldg, 3400 Spruce St, Philadelphia, PA 19104. From the 1999 RSNA scientific assembly. Received February 23, 2001; revision requested April 12; revision received October 26; accepted December 12. Supported in part by DAMD17-00-1-0406. **Address correspondence to** S.P.W.

Author contributions:
Guarantors of integrity of entire study, all authors; study concepts and design, all authors; literature research, S.P.W.; experimental studies, all authors; data acquisition and analysis/interpretation, all authors; manuscript preparation, S.P.W.; manuscript definition of intellectual content, editing, revision/review, and final version approval, all authors.

Microcalcifications in Breast Tissue Phantoms Visualized with Acoustic Resonance Coupled with Power Doppler US: Initial Observations[1]

Calcium carbonate particles embedded in gelatin and turkey breast tissues were visualized with acoustic resonance imaging and power Doppler ultrasonography. Sonography revealed that the region of color level detection corresponded to the location of the calcium carbonate particles. Correlation between color level detection and the location of the particles was confirmed on radiographs of the specimens obtained at core needle biopsy performed through the region of color level detection.

It is estimated that ductal carcinoma in situ represents 20%–30% of breast carcinomas detected at screening mammography (1). Since the 1970s, the detection rate of ductal carcinoma in situ has steadily increased with the wider use of screening mammography. The detection rate for women younger than 50 years was 2.3 cases per 100,000 women in the 1970s and increased to 6.2 cases per 100,000 women by the 1990s (2). More dramatically, in the group of women older than 50 years, the rate has increased from 14.3 to 54.6 per 100,000 (2) in the same period.

Frequently, ductal carcinoma in situ manifests only as calcifications without an associated mass (3). Because ductal carcinoma in situ represents as much as half of mammographically depicted cancers (3), it would be efficacious to image microcalcifications with as many modalities as possible to allow flexibility in imaging-guided biopsy. Currently, even with all the technical advances in breast imaging, including magnetic resonance imaging, scintigraphy, and ultrasonography (US), mammography is the only reliable method to help detect, characterize, and localize microcalcifications for biopsy.

We have developed a technique in which acoustic resonance is used to visualize microcalcifications. Acoustic resonance is used on the basis of the size of the microcalcifications and the binding strength with the surrounding tissues in which they are embedded. When subjected to a wide frequency range, particles of different sizes will resonate at different frequencies given the same binding environment. "Tuning" to the appropriate frequency range would make it possible to selectively visualize microcalcifications of varying sizes. The purpose of our study was to evaluate US coupled with acoustic resonance to demonstrate small calcified particles for targeting and biopsy.

Materials and Methods

Phantoms

Gelatin phantoms were constructed by using a mixture of water, gelatin, and glycerol with uniformly dispersed oil-lecithin emulsion (particle diameter, 0.2–2.0 μm). The suspension was placed in a mold and refrigerated until a solid state was reached. Calcium carbonate particles 400–800 μm in diameter were suspended in the gelatin phantom in an area 1.0–1.5 cm in diameter. The phantom was kept refrigerated until use, at which time it was removed from the mold. Ten phantoms were made.

Twelve tissue phantoms were made from boneless turkey breast. The turkey breast was dissected along the tissue planes, and 400–800-μm-diameter calcium carbonate particles mixed in acoustic cou-

pling gel were embedded carefully to avoid air trapping. The region of the calcium carbonate particles ranged from 1.5 to 2.0 cm in diameter

Imaging: US Coupled with Acoustic Resonance

Imaging was performed (S.P.W. or C.S., with the assistance of J.A.P.) by using gray-scale and power Doppler US coupled with acoustic resonance (Logic 700; GE Medical Systems, Milwaukee, Wis). A variable 10–13-MHz transducer was used. All the gelatin and tissue phantoms were scanned. The phantoms were imaged with B-mode US and power Doppler US, while the particles were resonated from 50 to 500 Hz. The frequency that corresponded to the maximum color level detection was noted.

The frequency used to excite the particles into resonance was emitted from a thin (5-mm) lightweight (13-g) piezoelectric speaker element with the capability to transmit low-frequency vibrations from 50 Hz to 2 kHz. The device was housed in a fiberglass case. The piezoelectric vibrator was designed for 8 Ω of impedance to be driven by an audio amplifier. The vibrator was specially designed by the biomedical medical instrumentation group at our university; they specialize in building custom instruments, and this vibrator was approved for human use by the university institutional review board. The disk was coupled with US gel (E-Z-Gel; E-Z-Em, Westbury, NY) and placed adjacent to the tissue to be scanned. The images were videotaped for analysis.

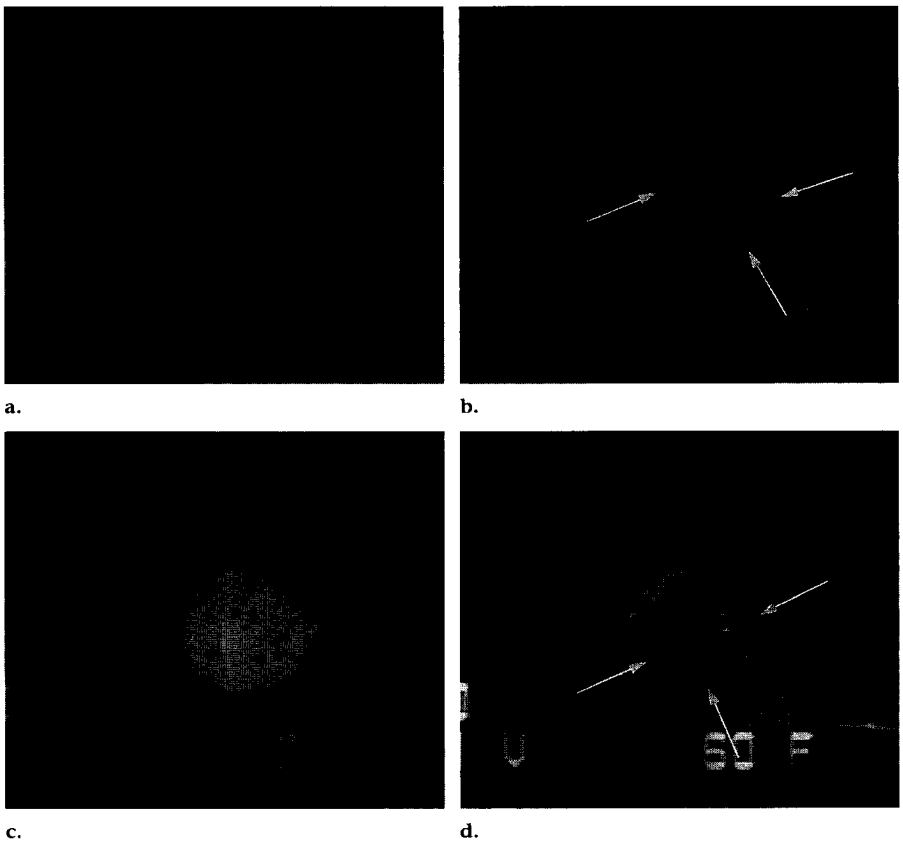

Figure 1. Color Doppler US images of gelatin phantoms evaluated with acoustic resonance and power Doppler US. Color is represented in gray scale. **(a)** Echogenic calcium carbonate particles are clearly visible in the gelatin phantom. **(b)** As the frequency is gradually increased to 100 Hz, the color pixels are seen as gray areas (arrows) in the region of the calcium carbonate particles. The pixels in this region were seen in color on the original images. **(c)** At 210 Hz, the entire region of the calcium carbonate particles is filled in with color pixels. **(d)** At 400 Hz, only a few color pixels (arrows) are seen.

Image Analysis

The videotaped images were subsequently analyzed. Imaging time for each scan was approximately 2 minutes. At the video frame rate of 30 images per second, approximately 120 × 30, or 3,600, images were generated. An algorithm was developed to reduce the data by sorting the images on the basis of the frequency of the vibration. These images were subsequently used in a computer program developed in our laboratory to analyze the vibrational response of the microcalcifications.

Color was analyzed for each image: Mean color level, percentage of fractional area of color, and color-weighted fractional area were computed. To determine the mean color level, the color palate on the image was read by the computer and divided equally on a scale of 0–100. With this scaling system, the computer constructed a lookup table for hue, saturation, and brightness values for the colors in the palette bar. Next, the computer identified colored pixels on the image and used the lookup table to assign a color value to each pixel in the region of interest. The color level of the pixels in the region of interest was summed and divided by the number of color pixels to calculate the mean color level. The percentage of fractional area of color was defined as the area covered by colored pixels divided by the area of the region of interest, multiplied by 100%. Color-weighted fractional area was defined as the mean color level multiplied by the percentage of fractional area of color, all divided by 100, and indicated the presence of net motion in the region of interest. Each parameter was plotted with respect to the frequency range.

Biopsy

All the gelatin and tissue phantoms were scanned from 50 to 500 Hz. The location where the maximum color level was detected and the corresponding frequency were noted. To demonstrate that the area of color level detection in the phantoms corresponded to the calcium carbonate particles, biopsy was performed through the region of color detection level. A 14-gauge disposable core biopsy needle (Monopty Biopsy Instrument; Bard, Covington, Ga) was used to perform biopsy in the region of interest during in real-time scanning by using power Doppler US coupled with acoustic resonance imaging. Approximately seven to 10 samples were obtained for each phantom. The core biopsy samples were placed in a core needle biopsy specimen container (Beekley, Bristol, Conn). Radiography of the specimens (alpha RT; Instrumentarium, Milwaukee, Wis) was performed at 22 kVp and 6 mAs, with magnification of 1.8, to confirm that the biopsy target, the region of depiction at

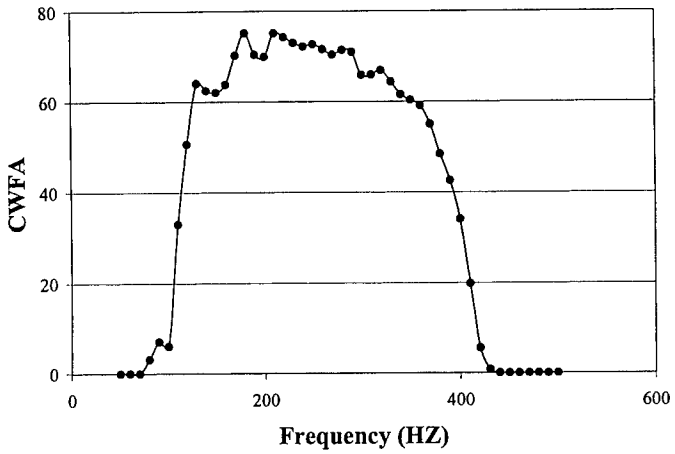

a.

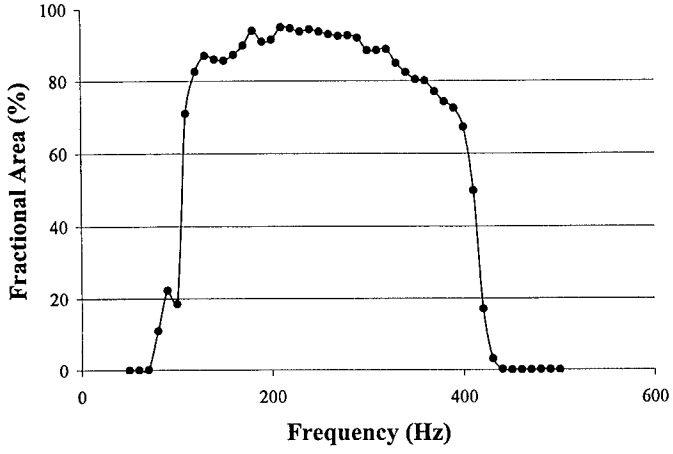

b.

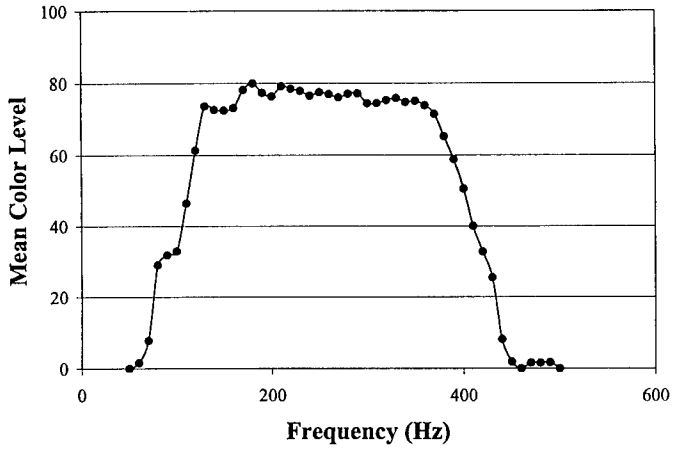

c.

Figure 2. Graphs plot (a) color-weighted fractional area *(CWFA)*, (b) percentage of fractional area, and (c) mean color level versus frequency in the gelatin phantom. Detection levels at power Doppler US increase, then plateau, and then rapidly decrease relative to frequency.

power Doppler US, corresponded to the calcium carbonate particles.

Results

Gelatin Phantom

The calcium carbonate particles were readily visible as white particles in all the gelatin phantoms at B-mode US. Figure 1a shows one of the phantoms. The calcium carbonate particles were readily visible in all 10 specimens. With power Doppler US evaluation, a gradual increase in color level detection was seen in the region of the calcium carbonate particles (Fig 1b). The maximum detection level was reached and then plateaued at frequencies of 200–380 Hz (Fig 1c). This plateau was followed by a gradual decrease in the color level detection (Fig 1d). This trend in color level detection was seen in all the gelatin phantoms evaluated. As seen in Figure 1, there was a minimal color level detected outside the region of the calcium carbonate particles. Graphs of mean color level, percentage of fractional area of color, and color-weighted fractional area versus frequency demonstrate the results seen on the static images in Figure 1, that is, a gradual increase in depiction level, followed by a decrease (Fig 2).

Turkey Phantom

The turkey phantom was also imaged with B-mode US and power Doppler US. In all 12 turkey phantoms, unlike in the gelatin phantoms, the calcium carbonate particles were not as readily visible at B-mode US before use of acoustic resonance imaging coupled with power Doppler US (Fig 3a). When the turkey phantom was imaged with power Doppler US coupled with acoustic resonance imaging, a gradual increase in color level detection was seen, a peak was reached, and a decrease followed (Fig 3b–3d). Similar findings in power Doppler detection were seen in all the turkey phantoms evaluated.

Biopsy Results

The radiograph of a specimen is shown in Figure 4. All radiographs of the specimens depicted the calcium carbonate particles in the specimens.

Discussion

The concept of acoustic resonance imaging is relatively new. There is a large body of literature that reports various modes of US imaging to characterize motion and elasticity of soft tissues induced by external vibrations or due to natural motion (4–8). None of these authors deal with the issue of detection of microcalcifications, nor do they use the concept of acoustic resonance as a means to identify the properties of inhomogeneities in the tissue. Our goal was to be able to visualize the resonance motion of inhomogeneities relative to that of the surrounding tissue.

The 400–800-μm calcium carbonate particles were excited into resonance when exposed to low-frequency vibrations from 50 to 500 Hz. The vibrations were of low amplitude, with no known harmful side effects. When the particles were in resonance and combined with power Doppler US, the calcium carbonate particles were expected to demonstrate a color level relative to the degree of resonance. At maximal resonance, there would be maximal color level detection. The frequency at which maximal resonance is demonstrated depends on the size of the microcalcifications and the binding properties between the tissue

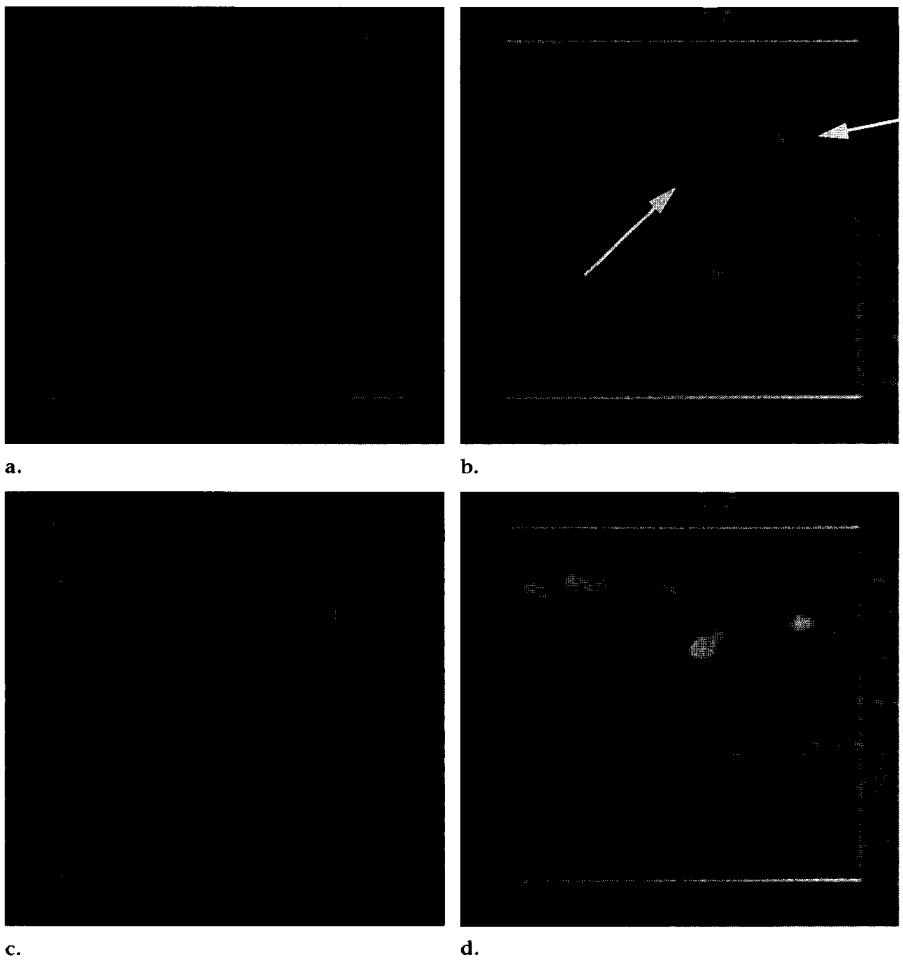

Figure 3. (**a**) US scan depicts a turkey breast phantom. Calcium carbonate particles are not as obvious as they are in the gelatin phantom. Color is represented in gray scale. (**b–d**) Power Doppler US scans coupled with acoustic resonance depict some color pixels in the region of the calcium carbonate particles (arrows) at 155 Hz (**b**); the number of color pixels continues to increase at 270 Hz (**c**); followed by a decrease at 355 Hz (**d**).

and the microcalcifications, which is demonstrated with the phantom models as shown in Figures 1 and 3. Graphs of the mean color level, percentage of fractional area of color, and color-weighted fractional area versus frequency demonstrate an increase in power Doppler US depiction level, followed by a plateau, then a decrease. The plateau, seen in the curves, may represent the particles of different sizes reaching resonance over a different range of frequencies.

In the simple gelatin phantom, the microcalcifications were visible without power Doppler US, which allowed direct correlation between the location of the particles and the area of color-level depiction. Unlike the homogeneous background of the gelatin phantom, the turkey phantom more closely approximates human breast tissue, with muscle striations and specular interfaces similar to the appearance of Cooper ligaments and other specular reflectors in human glandular tissue. Therefore, the location of the calcium carbonate particles is not obvious until power Doppler US coupled with acoustic resonance imaging is used. Core biopsy was performed in the area where color level was detected in both types of phantoms, and radiography of the specimens was performed. Findings on the radiographs of the specimens confirmed that the region of color level detection corresponded to the calcium carbonate particles.

There are multiple potential applications for this method. Once the microcalcifications are detected at US, biopsy could be performed with this dynamic imaging guidance. Results of various studies have demonstrated the cost-effectiveness of core needle biopsy compared with excisional biopsy (9–12) or US-guided core needle biopsy versus stereotactic core needle biopsy (13). With the ability to perform biopsy with vacuum assistance and US guidance, this method would allow performance of biopsy in calcifications by using US and possibly dynamic visualization of the extraction of calcifications, which would allow con-

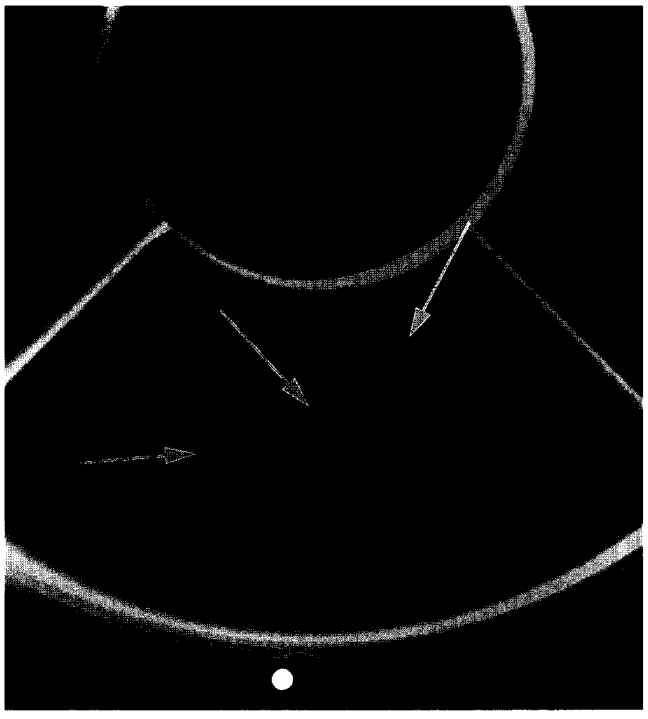

Figure 4. Radiograph of a specimen depicts calcium carbonate particles (arrows) in the core biopsy samples.

firmation of targeting and, conceivably, a procedure time shorter than that for stereotactic core needle biopsy. Currently, sonographically guided biopsy is not always feasible because calcifications cannot always be definitively visualized with US alone.

We have shown that power Doppler US coupled with acoustic resonance imaging has the ability to demonstrate microcalcifications in phantom models. Future studies are needed to develop this technique for use in patients. US evaluation may be performed in women prior to conventional stereotactic or excisional biopsy. Correlation between particle size, peak resonance, binding properties, and pathologic results may provide beneficial information. Analysis of acoustic resonance properties may help determine the strength of adhesion between the calcium deposits and the surrounding tissues. Such forces are likely to be related to the molecular characteristics of the deposits and the mechanisms that cause calcifications to develop at specific sites in the tissues. Measurement of adhesive forces with acoustic resonance, in conjunction with morphologic parameters detected at mammography, may help characterize calcifications.

References

1. Kopans D. Pathologic, mammographic, and sonographic correlation. In: Kopans D, ed. Breast imaging. 2nd ed. Philadelphia, Pa: Lippincott-Raven, 1998; 511–615.
2. Morrow M, Schnitt SJ, Harris JR. In situ carcinomas. In: Harris JR, Lippman ME, Morrow M, Hellman S, eds. Diseases of the breast. Philadelphia, Pa: Lippincott-Raven, 1996; 355–373.
3. Ernster VL, Barclay J, Kerlikowske K, et al. Mortality among women with ductal carcinoma in situ of the breast in the population-based surveillance, epidemiology and end results program. Arch Intern Med 2000; 160:953–958.
4. Dickenson RJ, Hill CR. Measurement of soft tissue motion using correlation between A-scans. Ultrasound Med Biol 1982; 8:263–271.
5. Wilson LS, Robinson DE. Ultrasonic measurement of small displacements and deformations of tissue. Ultrason Imaging 1982; 4:71–82.
6. Lerner RM, Huang SR, Parker KJ. Sonoelasticity images derived from ultrasound signals in mechanically vibrated tissues. Ultrasound Med Biol 1990; 16:231–239.
7. Adler RS, Rubin JM, Bland PH, et al. Quantitative tissue motion analysis of digitized M-mode images: gestational differences of fetal lung. Ultrasound Med Biol 1990; 16:561–566.
8. Ophir J, Cespedes I, Ponnekanti H, et al. Elastography: a quantitative method for imaging the elasticity of biological tissues. Ultrason Imaging 1991; 13:111–134.
9. Hillner BE, Bear HD, Fajardo LL. Estimating the cost-effectiveness of stereotaxic biopsy for nonpalpable breast abnormalities: a decision analysis model. Acad Radiol 1996; 3:351–360.
10. Liberman L, Fahs MC, Dershaw DD, et al. Impact of stereotaxic core breast biopsy on cost of diagnosis. Radiology 1995; 195:633–637.
11. Lee CH, Egglin TK, Philpotts L, et al. Cost-effectiveness of stereotactic core needle biopsy: analysis by means of mammographic findings. Radiology 1997; 202: 849–854.
12. Yim JH, Barton P, Weber B, et al. Mammographically detected breast cancer: benefits of stereotactic core versus wire localization biopsy. Ann Surg 1996; 223: 688–697.
13. Liberman L, Feng TL, Dershaw DD, et al. US-guided core breast biopsy: use and cost-effectiveness. Radiology 1998; 208: 717–723.